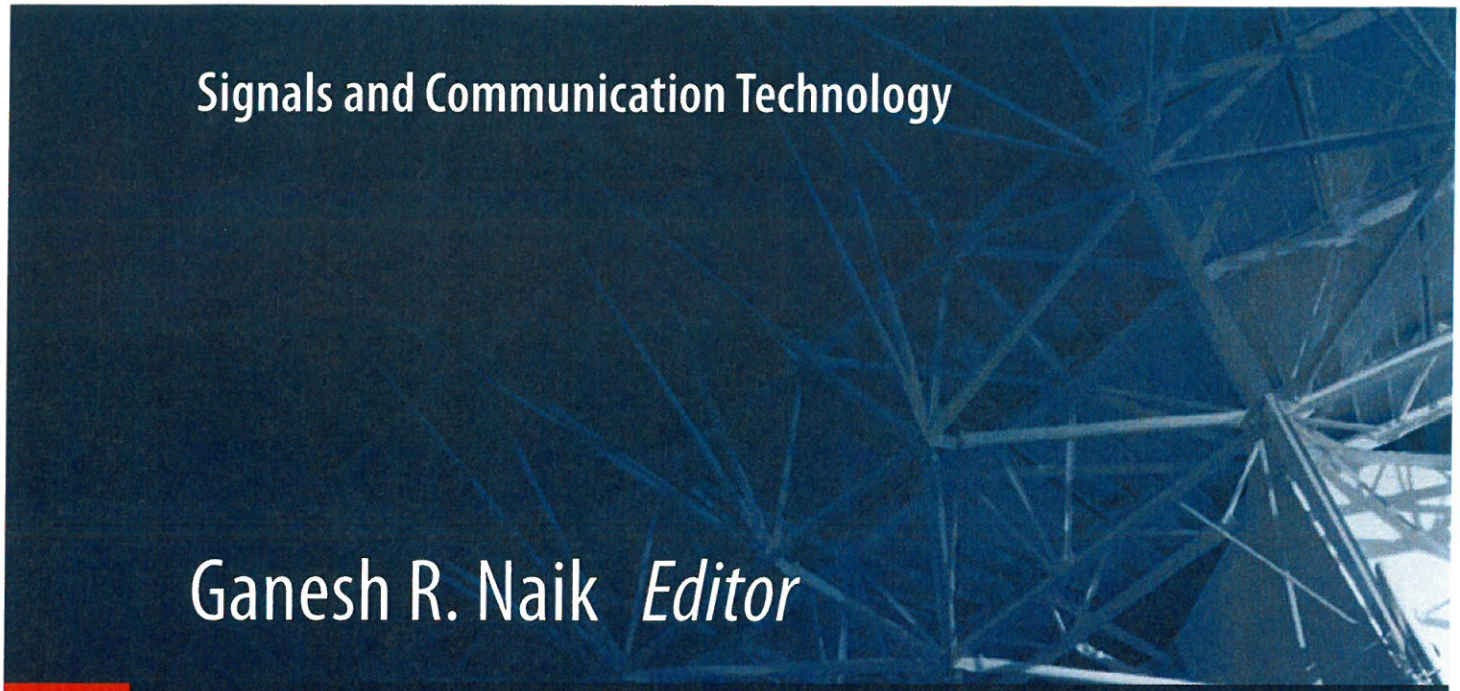
Signals and Communication Technology



Ganesh R. Naik *Editor*

Non-negative Matrix Factorization Techniques

Advances in Theory and Applications

Springer

Chapter 7
NMF in MR Spectroscopy

T. Laudadio, A.R. Croitor Sava, Y. Li, N. Sauwen, D.M. Sima and S. Van Huffel

Abstract Nowadays, magnetic resonance spectroscopy (MRS) represents a powerful nuclear magnetic resonance (NMR) technique in oncology since it provides information on the biochemical profile of tissues, thereby allowing clinicians and radiologists to identify in a non-invasive way the different tissue types characterising the sample under investigation. The main purpose of the present chapter is to provide a review of the most recent and significant applications of non-negative matrix factorisation (NMF) to MRS data in the field of tissue typing methods for tumour diagnosis. Specifically, NMF-based methods for the recovery of constituent spectra in ex vivo and in vivo brain MRS data, for brain tissue pattern differentiation using magnetic resonance spectroscopic imaging (MRSI) data and for automatic detection and visualisation of prostate tumours, will be described. Furthermore, since several NMF implementations are available in the literature, a comparison in terms of pattern detection accuracy of some NMF algorithms will be reported and discussed, and the NMF performance for MRS data analysis will be compared with that of other blind source separation (BSS) techniques.

Keywords NMF · MRS · MRSI · Nosologic imaging · Brain tumours · Prostate cancer

T. Laudadio (✉)
Istituto per le Applicazioni del Calcolo "M. Picone" (IAC), Consiglio Nazionale delle Ricerche, Bari, Italy
e-mail: t.laudadio@ba.iac.cnr.it

A.R. Croitor Sava · N. Sauwen · D.M. Sima · S. Van Huffel
Department of Electrical Engineering (ESAT), STADIUS Center for Dynamical Systems, Signal Processing and Data Analytics, KU Leuven, Leuven, Belgium

A.R. Croitor Sava · N. Sauwen · D.M. Sima · S. Van Huffel
iMinds Medical Information Technologies, Leuven, Belgium

Y. Li
School of Electronic Engineering, University of Electronic Science and Technology of China, Chengdu, China

© Springer-Verlag Berlin Heidelberg 2016

G.R. Naik (ed.), *Non-negative Matrix Factorization Techniques*,
Signals and Communication Technology, DOI 10.1007/978-3-662-48331-2_7

t.laudadio@ba.iac.cnr.it

7.1 Introduction

NMR is widely used in oncology as a non-invasive diagnostic tool to detect the presence of tumour regions in the human body. One application of NMR is magnetic resonance imaging (MRI), which is applied in routine clinical practice to localise tumours and determine their size. MRI is able to provide an initial diagnosis, but its ability to delineate anatomical and pathological information is significantly improved by its combination with another NMR application, known as MRS. The latter provides information on the biochemical profile of tissues by exhibiting peaks at specific frequencies representing the molecular composition of the tissue under investigation, which appear in the MR signal as a spectrum of resonances. MRS can thus provide relevant information on cancer metabolism, allowing clinicians and radiologists to identify the different tissue types characterising the considered sample, and to study the biochemical changes underlying a pathological condition [1–3]. The simultaneous acquisition of several MR signals to produce spatially localised spectra within the organ of interest is referred to as MRSI. The analysis of MRS(I) data could represent a powerful diagnostic tool as it could be used to detect and localise the presence of a tumour, to classify its nature and to study the tumour metabolism in order to evaluate the response to possible therapies [4, 5]. Nevertheless, the clinical application of MRS(I) is still difficult because the analysis of MRS(I) data requires a lot of expertise as well as time-demanding, user-dependent and sophisticated processing procedures aimed at improving the quality of the acquired data and at extracting the information of interest. Therefore, automatic, accurate and efficient processing algorithms are needed in order to introduce MRS(I) in daily clinical practice.

Recently, NMF [6] has successfully been applied to brain as well as to prostate MRS(I) data in order to extract characteristic metabolic tissue patterns and to describe their contribution (abundance) to the profile of each spectrum. In particular, the studies described in [7–14] show that the application of NMF allows to overcome some of the main limitations that still affect most tissue segmentation and classification techniques of MRS(I) data available in the literature, i.e., need of prior knowledge, lack of automation and inability to properly describe tissue mixtures since each tissue volume element (or, equivalently, voxel), where the MRS signal is measured, is only labelled as being tumourous or non-tumorous.

On the opposite, extensive simulation and in vivo studies show that the proposed NMF-based methods are able to automatically detect accurate patterns for tumour, healthy and other interesting tissues without the need of any prior tissue model. Furthermore, they do not require massive MRS(I) data pre-processing aimed at removing artefacts, instrumental limitations, noise, etc., since NMF is able to detect the presence of uninteresting components as separate sources [13, 14].

The main purpose of the present chapter is to provide a review of the most recent and significant applications of NMF to MRS(I) data in the field of tissue typing methods for tumour diagnosis. Specifically, NMF-based methods for the recovery of constituent spectra in ex vivo and in vivo brain MRS data [7, 8], for brain tissue pattern differentiation using MRSI data [9–12], and for automatic detection and

t.laudadio@ba.iac.cnr.it

visualisation of prostate tumours [13, 14], will be described. Furthermore, since several NMF implementations are available in the literature, a comparison in terms of pattern detection accuracy of some NMF algorithms will be reported and discussed, and the NMF performance for MRS data analysis will be compared with that of other BSS techniques.

7.2 NMF: Basic Principles and Its Application to Ex Vivo and In Vivo Brain MRS Data for Tissue Pattern Extraction

NMF is a BSS technique imposing non-negative constraints on the extracted sources and corresponding weights. Specifically, given a non-negative matrix $X \cdot R^{m \times n}$, and an integer k $(0 < k < min(m, n))$, two non-negative matrices $W \cdot R^{m \times k}$ and $H \cdot R^{k \times n}$, minimising the functional

$$f(W, H) = \frac{1}{2} \|X - WH\|_F^2 \tag{7.1}$$

are estimated, where the subscript F stands for Frobenius norm [15]. It is worth noticing that, given the non-convex nature of $f(W, H)$, its minimisation may lead to the estimation of local minima and does not admit unique solution [16]. In order to deal with such a problem, a variety of NMF algorithms have been proposed in the literature and comparative studies of such implementations in terms of performance are often reported in theoretical as well as applicative studies [17]. Also in this chapter several NMF implementations will be considered and their performance will be compared in terms of source detection accuracy.

7.2.1 Application of NMF to Brain HR-MAS Data

In [7], NMF was applied to ex vivo high-resolution magic angle spinning (HR-MAS) spectra in order to extract characteristic tissue patterns of brain glial tumours and to quantify their contribution to each of the given spectra. HR-MAS represents an additional NMR spectroscopy technique that allows the identification of a higher number of important metabolites compared to standard MRS. For this reason, HR-MAS spectra are frequently used for metabolic analysis of tissue samples and, in particular, they have recently been used for brain tissue characterisation and tumour diagnosis [18], thereby representing a valuable alternative to histopathology which is time and effort expensive.

In general, brain glial tumours are heterogeneous and, for the high grade cases, they are also infiltrative. Therefore, HR-MAS spectra profiles belonging to the same brain tumour tissue type could show a significant variability [19]. Specifically, glial

t.laudadio@ba.iac.cnr.it

tumours might present contribution from the following different tissues: necrosis, highly cellular cells, healthy tissue and border tissue that contains tumour and apparently healthy brain cells. The observed spectra can then be considered a combination of different constituent sub-spectra, also referred to as sources, and the overall contribution of a tissue type to a spectrum is proportional to its abundance, i.e., to its proportion in the entire mixed tissue sample. As suggested in [7], the estimation of the aforementioned HR-MAS sub-spectra and corresponding abundances could be formulated as a BSS problem. More precisely, given n HR-MAS spectra, each consisting of m data points, they could be stacked as column vectors in an $m \times n$ matrix X. Then, the observed spectra can be described as follows:

$$X = WH + N \tag{7.2}$$

where the columns in W represent the unknown constituent tissue sources and the rows in H represent the corresponding concentrations or abundances. N represents additive noise. Given the non-negative nature of the HR-MAS data in [7], consisting of magnitude spectra, and the possible correlation that could characterise the profiles of the constituent tissues, two different NMF implementations were considered: an NMF algorithm exploiting sparsity constraints (NMFSC) [20], and one based on a convex analysis of mixtures of non-negative sources (CAMNS) [21]. Furthermore, the results obtained by NMFSC and CAMNS were compared with those ones provided by non-negative independent component analysis (nICA) [22], an additional non-negative BSS technique that imposes sources to be non-negative as well as mutually independent.

The aforementioned BSS algorithms were applied to HR-MAS spectra of brain tissue samples from 52 patients affected by a glial tumour with different degrees of malignancy. Such data were provided by the database of an European project entitled eTUMOUR (URL: http://www.etumour.net/). More precisely, the above algorithms were applied to the full HR-MAS spectra (consisting of 716 data points) as well as to metabolic feature vectors of different lengths ($n = 19$ and $n = 8$) extracted from the above spectra by peak integration [23] in order to study the influence of the input space (X matrix) on the algorithm performance. Specifically, the feature vector of length $n = 19$ contained all the estimated metabolite concentrations, and the one of lengths $n = 8$ was obtained by the previous vector by selecting only the concentrations of the most representative metabolites as reported in [19, 24].

To evaluate the source detection accuracy of NNMFSC, CAMNS and nICA, the correlation coefficient between the results provided by the above BSS techniques and reference tissue models provided by histopathology were computed. In particular, the correlation coefficients obtained by setting $k = 3$ (i.e., number of assumed pure tissues) for the glioblastoma (GBM) group when considering the different input spaces are displayed in Table 7.1. Such values show that NNMFSC and CAMNS provide a very accurate necrosis tissue source, independently of the input space dimension. A similar value is obtained by nICA as well when applied to the input space consisting of feature vectors of length $n = 8$. Concerning the detection of the tumour tissue source, all methods are less accurate than in the previous case and all

t.laudadio@ba.iac.cnr.it

Table 7.1 Correlation coefficients between the obtained tissue sources and the reference tissue models for different input feature spaces [7]

	$n = 716$	$n = 19$	$n = 8$
NNMFSC			
Necrotic	0.97	0.97	0.99
Tumour	0.69	0.68	0.72
Border	0.91	0.92	0.92
CAMNS			
Necrotic	0.98	0.99	0.97
Tumour	0.62	0.61	0.71
Border	0.89	0.54	0.88
nICA			
Necrotic	0.81	0.93	0.98
Tumour	0.68	0.67	0.73
Border	0.83	0.51	0.68

of them perform best when applied to the aforementioned input space. Finally, the best border tissue source is provided by NNMFSC. Figure 7.1 shows the three tissue sources obtained by NNMFSC when applied to the magnitude spectra (left column) along with the corresponding reference tissue models provided by histopathology (right column). Looking at the overall performance of the considered methods, the

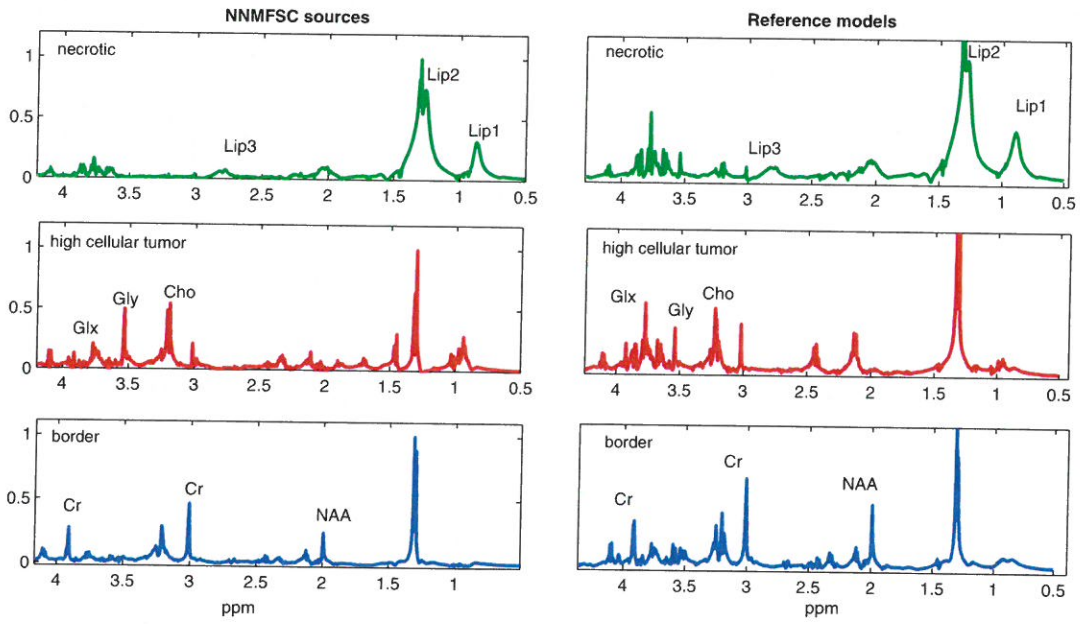


Fig. 7.1 *Left column* tissue sources obtained by NNMFSC when applied to magnitude spectra. *Right column* reference tissue models provided by histopathology. Lip1, Lip2 and Lip3 stand for lipids, Glx for glutamine + glutamate, Gly for glycine, Cho for choline and Cr for creatine [7]

t.laudadio@ba.iac.cnr.it

results show that the sources provided by NNMFSC are the closest ones to the reference tissue models. CAMNS performs quite similarly to NNMFSC, probably because the two methods rely on the same principles, i.e., they impose sparsity and do not require sources to be mutually independent or uncorrelated. Still, with CAMNS, the assumption of sparsity is too strong since when a source, such as border and highly active tumour tissues, exhibits a non-zero value for a feature, all the other sources must have a zero value. On the other hand, this assumption is appropriate when considering the necrotic tissue source, which is characterised by high levels of lipids, while the other metabolic components are mostly embedded in noise and, therefore, are close to zero. Finally, nICA imposes the sources to be mutually independent and, consequently, uncorrelated. Such an assumption is too strong and not suitable for the considered data analysis since, as already described above, HR-MAS spectra from different tissue types can be correlated.

7.2.2 Application of NMF to Brain MRS Data

Recently, in [8] NMF has also been applied to single voxel brain MRS data measured in patients affected by brain tumour. The studies were carried out on data provided by an international multi-centre database [25] developed in the context of the European research project entitled INTERPRET [26]. In [8], the performance of a variety of NMF methods was investigated and compared when applied to the aforementioned MRS data to detect the main constituent sub-spectra representing characteristic pure tissue types in brain tumours. Furthermore, the NMF method characterised by the best performance in terms of tissue pattern detection was afterwards exploited, as pre-processing step, for dimensionality reduction in classical supervised classification algorithms commonly applied to MRS data.

The above studies show that the best performance was obtained by an NMF implementation known as CONVEX-NMF [27]. This algorithm, differently from the conventional ones available in the literature, imposes non-negative constraints only on the mixing matrix H, while entries in X and W are allowed to assume positive as well as negative values. Such a property makes CONVEX-NMF suitable for processing data of mixed sign. Indeed, if the given MRS data contain negative peaks, as those ones considered in [8], the detected sources will contain negative peaks as well, thereby avoiding the loss of important biochemical information which normally occurs when making the data non-negative prior to the application of conventional NMF methods. For instance, when processing long-echo time spectra, CONVEX-NMF allows the detection of some important metabolites, such as lactate, alanine and glutamine + glutamate, which play a crucial role in discriminating the different brain tumour types. Such a discrimination would not be possible by applying NMF algorithms imposing non-negative constraints on H as well as on X and W, since they usually truncate negative values occurring in the estimated sources to zero, with the consequent loss of information related to relevant negative peaks.

t.laudadio@ba.iac.cnr.it

Concerning the application of CONVEX-NMF as pre-processing step for dimensionality reduction in supervised classification, the studies described in [8] show that it provides, in a fully unsupervised way, results comparable to and, in some cases, more accurate than those ones obtained by applying standard supervised classification approaches reported in the literature, such as for instance the one based on combining principal component analysis [28] with linear discriminant analysis [29].

7.3 NMF Applied to Brain MRSI Data for Tissue Pattern Differentiation

In [9], CONVEX-NMF has also been applied to brain MRSI data measured in tumour-bearing mice in order to extract sources describing characteristic pure tissues and, after determining the tumour tissue pattern, to delimit and visualise the tumour area in a fully unsupervised mode. As in [8], the performance of CONVEX-NMF has been compared with that of other NMF implementations, and the results of such studies confirm that CONVEX-NMF performs best in terms of source detection, thereby providing an accurate tumour region delimitation. The method proposed in [9] represents a significant achievement in tumour detection and visualisation since, differently from other approaches available in the literature, it is unsupervised and, therefore, does not require any label for tumour or normal tissue to find the desired sources. Nevertheless, it only allows the separation of tumour versus non-tumour tissue, without taking into account that the detection of other characteristic pure tissues is of crucial importance for therapy planning. Furthermore, up to our knowledge, the method has not been tested on MRSI data measured in human brain.

Alternative applications of NMF to human brain MRSI data have been proposed in [10–12]. More precisely, in these studies NMF has been embedded into a hierarchical scheme aimed at extracting the constituent sub-spectra from the given data and to visualise their distribution. It is worth highlighting that the hierarchical approaches proposed in [10–12] show significant differences. First of all, the studies described in [10] were carried out on long-echo time signals, while short-echo time signals were considered in [11, 12]. Second, they made use of different NMF algorithms. Specifically, in [10] the authors proposed a constrained version of NMF which forces negative amplitude values, occurring in the recovered sources and abundance distributions, to be approximately equal to zero. In [11, 12], the hierarchical alternating least squares (HALS) algorithm [30–32] was considered since in a preliminary study it was proven to be superior to other NMF implementations when applied to simulated brain MRSI data [33]. Last but not the least, the main purpose of the algorithm proposed in [10] consisted in separating abnormal brain tissue from the normal one. However, it is well known that for GBMs there exist two distinct patterns for abnormal tissue, representing tumour and necrosis tissue. In [11], a novel hierarchical non-negative matrix factorisation (hNMF) method was developed in order to accurately estimate the three most important tissue patterns for GBMs (normal, tumour and necrosis). For shortness' sake, below only the latter algorithm is described.

t.laudadio@ba.iac.cnr.it

7.3.1 hNMF for GBM

Let us here assume that the model describing the data is (7.2). The algorithm hNMF consists in the following three main steps:

Step 1. First-level NMF: NMF is applied to the data matrix X by setting $k = 2$. Two spectral profiles and their corresponding h-maps (H_{normal} and $H_{abnormal}$) are recovered. The spectral sources obtained are automatically assigned to 'normal' and 'abnormal' tissue (W_{normal} and $W_{abnormal}$) based on the ratio between the metabolites N-acetylaspartate (NAA) and lipids (Lips) (where the values of NAA and Lips are estimated as the maximum intensity in the frequency regions around 2.01 and 1.3 ppm, respectively). The source with the higher NAA/Lips ratio corresponds to normal tissue and the source with the lower NAA/Lips ratio corresponds to abnormal tissue [34].

Step 2. Second-level NMF: NMF is performed with two sources repeatedly, on several sets of voxels, and the best result is chosen, as follows. Let us consider a variable threshold t on the magnitude of the $H_{abnormal}$ map, according to which a mask $f(t)$ is created, i.e. a selection of 'abnormal' voxels having values of $H_{abnormal}$ larger than t. For any fixed value of t, NMF with $k = 2$ is applied to the set of currently selected 'abnormal' spectra, leading to two sources, $W^1_{abnormal}(t)$ and $W^2_{abnormal}(t)$. In order to choose the best mask $f(\hat{t})$ from a set of gradually decreasing masks, a reasonable trade-off is sought, such that W_{normal}, $W^1_{abnormal}(\hat{t})$ and $W^2_{abnormal}(\hat{t})$ are mutually least correlated, i.e.

$$\hat{t} = \arg\min(corr1(t) + corr2(t) + corr3(t)) \tag{7.3}$$

where

$$\begin{aligned} corr1(t) &= corr(W_{normal}, W^1_{abnormal}(t)) \\ corr2(t) &= corr(W_{normal}, W^2_{abnormal}(t)) \\ corr3(t) &= corr(W^1_{abnormal}(t), W^2_{abnormal}(t)) \end{aligned} \tag{7.4}$$

and $corr(x, y) = \frac{(x-\bar{x})^T(y-\bar{y})}{\|x-\bar{x}\|\cdot\|y-\bar{y}\|}$ for any two vectors x and y of the same length, while $\bar{x}$ and $\bar{y}$ are the means of x and y, respectively.

The profiles $W^1_{abnormal}(\hat{t})$ and $W^2_{abnormal}(\hat{t})$ are automatically assigned to necrosis and tumour tissue ($W_{necrosis}$ and W_{tumour}) based on the choline (Cho)-to-Lips ratio (where such values are estimated as the maximum intensity in the frequency regions around 3.22 and 1.3 ppm, respectively). Based on previous studies [34], the source with the smaller Cho/Lips ratio is assigned to necrosis and the other is assigned to tumour.

Step 3. Non-negative least squares (NNLS) re-estimation: NNLS [35] is applied to the grid considered in Step 1 using the sources W_{normal}, W_{tumour} and $W_{necrosis}$ to re-estimate the corresponding h-maps.

t.laudadio@ba.iac.cnr.it

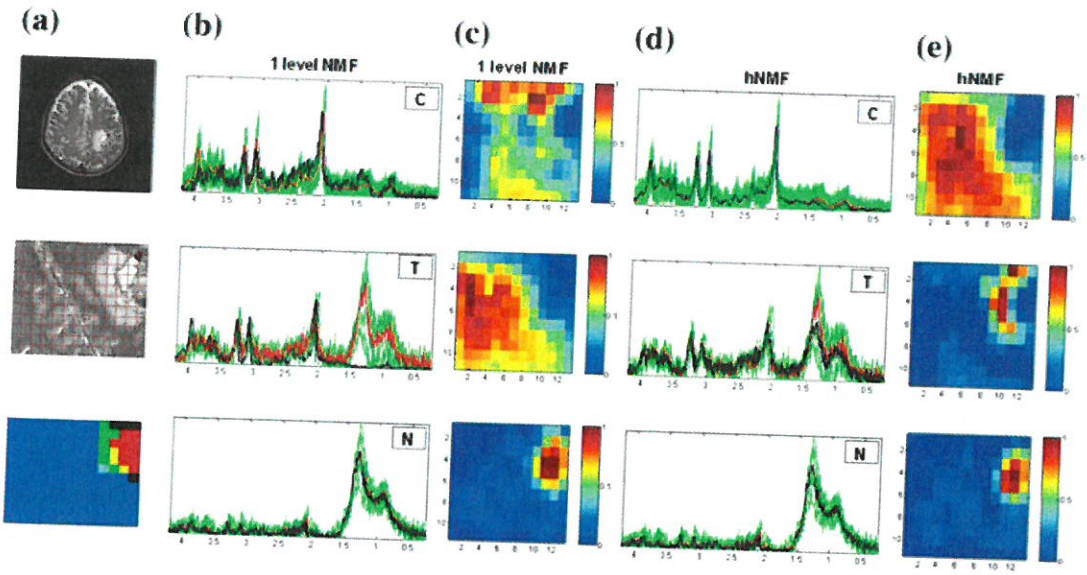


Fig. 7.2 Tissue pattern differentiation on 1H MRSI data from a patient with GBM: C, T and N represent normal, tumour and necrosis, respectively. **a** *First row* anatomical T2-weighted MR image. Clear tumour and necrosis regions are visible in the image. *Second row* selected voxels of interest. *Third row* expert labelling, where *red* indicates N, *yellow* indicates N/T, *green* indicates T, *cyan* indicates C/T, *blue* indicates C and *black* indicates spectra of poor quality. **b, c** Results of one-level NMF. **b** The recovered sources are shown in *black*. Spectra in *red* are the 'ideal' spectra according to expert labelling. Spectra in *green* show all the tissue-specific spectra labelled by the experts. **c** Corresponding h-maps for each spectral profile given in (**b**). **d, e** Results of hNMF. **d** The recovered sources for C, T and N are shown in *black*, overlaid over the 'ideal' spectra in *red*. Spectra in *green* show all the tissue-specific spectra labelled by the experts. **e** Corresponding h-maps which can be compared with the anatomical image and expert labelling [11]

The performance of the method was tested on simulated as well as on in vivo short-echo MRSI GBM data because GBM represents a very heterogeneous and aggressive brain tumour. Furthermore, it was compared with that of one-level NMF applied with $k = 3$, i.e. number of pure tissue patterns to be detected, and with expert labelling for the in vivo tests. As shown in Fig. 7.2, where the results obtained for an in vivo example are reported, hNMF significantly outperforms the one-level NMF approach in terms of tissue pattern detection and visualisation of the corresponding areas. The reason why the one-level NMF fails is probably due to the fact that the tissue-specific spectral profile of tumour is not sufficiently uncorrelated from a linear combination of the other patterns representing normal and necrosis tissue. On the opposite, hNMF looks for the three most distinct (but possibly correlated) tissue-specific spectral profiles by optimising a mask on the abnormal region, which is meant to exclude voxels containing a mixture of tumour and normal tissue patterns. The mixing coefficients are finally computed as the h-maps corresponding to each tissue pattern.

As already mentioned above, compared to the previous studies described in [10], hNMF presents several novelties: first of all, it was applied to short-echo time spectra that are able to provide more diagnostic information than long-echo time spectra, but are potentially more challenging because of the more complex spectral profiles;

t.laudadio@ba.iac.cnr.it

hNMF was applied directly to brain tissue data and was able to differentiate three tissue patterns instead of only two (i.e. normal and abnormal) in the region encompassing the tumour; in the hierarchical application of NMF described in [10], only a fixed threshold was used to generate a mask for data selection, while in [11] an adaptive threshold selection was carried out; the NNLS re-estimation, added as last step in hNMF, avoids the loss of information at the border between tissue patterns, which may otherwise occur as a result of thresholding. Finally, the potential of hNMF is not limited to tissue pattern differentiation of GBMs. In principle, it could be adapted to solve other problems requiring more than two sources or more levels.

Recently, as described in [12], an additional step has been introduced into hNMF aimed at providing unsupervised nosologic images, where all the tissues of interest are simultaneously visualised by means of different colours. More precisely, each h-map provided by Step 3 (normalised between 0 and 1) is encoded as a colour channel into an RGB image, thereby obtaining a single image where red, green and blue, respectively, represent necrosis, tumour and normal tissue, while their possible mixture represents mixed tissues. The mixed colours of nosologic images provide a way to interpret tumour infiltration.

7.4 NMF Applied to Prostate MRSI Data for Automatic Detection and Visualisation of Tumours

In [13, 14], preliminary studies have been carried out on the application of NMF to simulate as well as to in vivo three-dimensional 3 T long-echo MRSI prostate data in order to extract characteristic patterns for tumour and benign tissue and to visualise their spatial distribution. In particular, in [14], a hierarchical approach is proposed which differs from those ones applied to brain data in [10–12]. Indeed, since the detection of only two tissue patterns is generally required for prostate data, i.e., tumour and benign tissue, NMF could be directly applied to the MRSI data set by setting $k = 2$. Nevertheless, as shown by extensive simulation studies, performing only one NMF level with $k = 2$ does not provide reliable results. Higher quality tissue patterns are obtained by embedding NMF into the hierarchical scheme (HNMF) as described below:

- The MRSI data are arranged into a matrix X, containing spectra as columns, and NMF is applied to X by setting $k = 2$. Two source signals and their corresponding weights are obtained.
- The given MRSI voxels are divided into two new data sets by assigning each voxel to the source signal characterised by the maximum weight in that voxel.
- The procedure is repeated after building new matrices X from spectra pertaining to each of the subsets obtained above.

t.laudadio@ba.iac.cnr.it

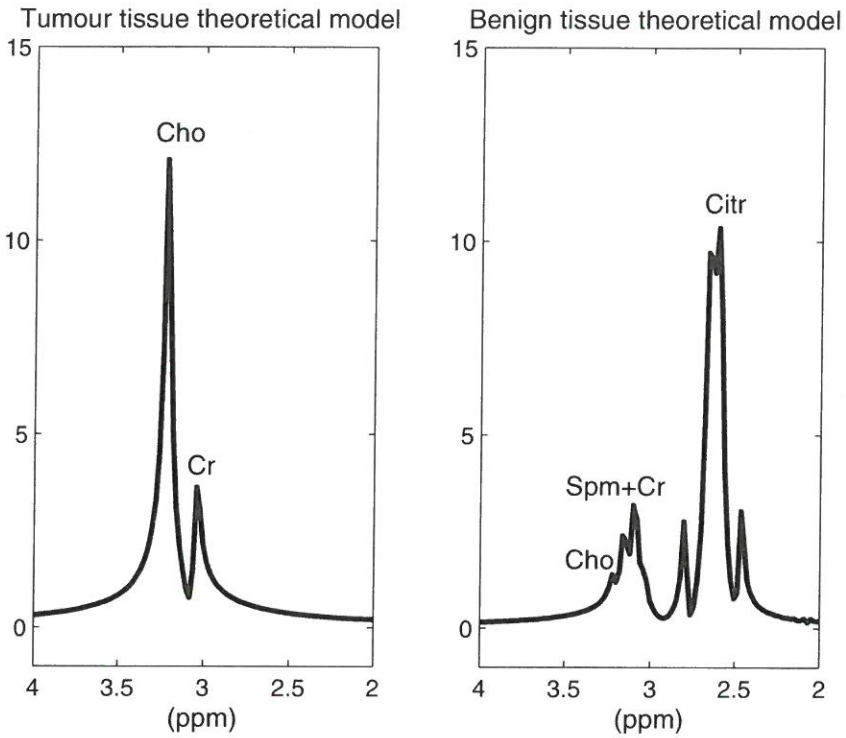


Fig. 7.3 Characteristic prostate magnitude spectra assumed for aggressive tumour tissue (*left*) and benign tissue (*right*). Cho stands for choline, Spm for spermine, Cr for creatine and Citr for citrate. The spectrum representing aggressive tumour tissue exhibits a high contribution of choline and no citrate, while benign tissue is represented by a spectrum characterised by a high citrate contribution, a small choline peak and contribution by the spermine model signal in the interval (3–3.2 ppm) [14]

In [14], several NMF levels, corresponding to increasingly finer partitions of the initial MRSI data, are applied, thereby obtaining a set of signal sources among which the two most significant ones, representing tumour and benign tissues, can be selected based on the prior knowledge that the choline-to-citrate ratio should be high for the source representing tumour tissue and low for the source representing benign tissue (see Fig. 7.3 where characteristic prostate magnitude spectra for aggressive tumour tissue (left) and benign tissue (right) are shown) [36].

As in [12], the selected tissue patterns can afterwards be encoded as different colour channels into an RGB image, and their spatial distribution can be visualised by means of different colours into a single image. As example, Fig. 7.4 shows a simulated dataset, consisting of a 10×10 grid of voxels (left picture), mimicking a prostate tumour. The contribution of the aggressive tumour model in each voxel of the above grid is displayed in the same figure (right picture). More precisely, the contribution of the tumour model to each spectrum, or voxel, in the grid can be retrieved from the colour bar displayed on the right-hand side of the image by looking for the value corresponding to the colour intensity present in the considered voxel.

t.laudadio@ba.iac.cnr.it

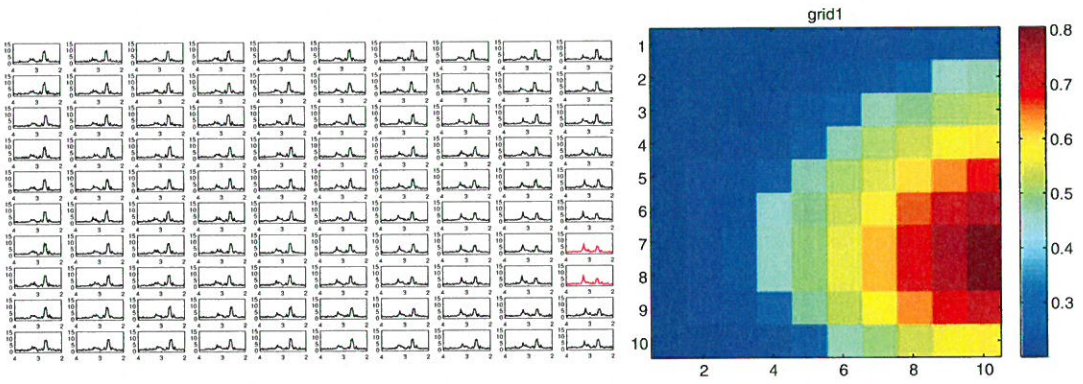


Fig. 7.4 *Left* simulated dataset. The most aggressive tumour spectra are displayed in *red* and they exhibit a low citrate contribution. *Right* tumour source spreading [14]

In Fig. 7.5, we first show the tumour and benign tissue patterns obtained by performing only one NMF level with $k = 2$ (left plots) and the final patterns provided by the hierarchical approach, i.e. by HNMF (right plots), for one simulation run when considering a medium noise level. The NMF implementation available in Matlab (a registered trademark of The MathWorks Inc., Natick, MA, USA), which is based on an alternating least squares scheme [17], and then here denoted by ALS, was applied.

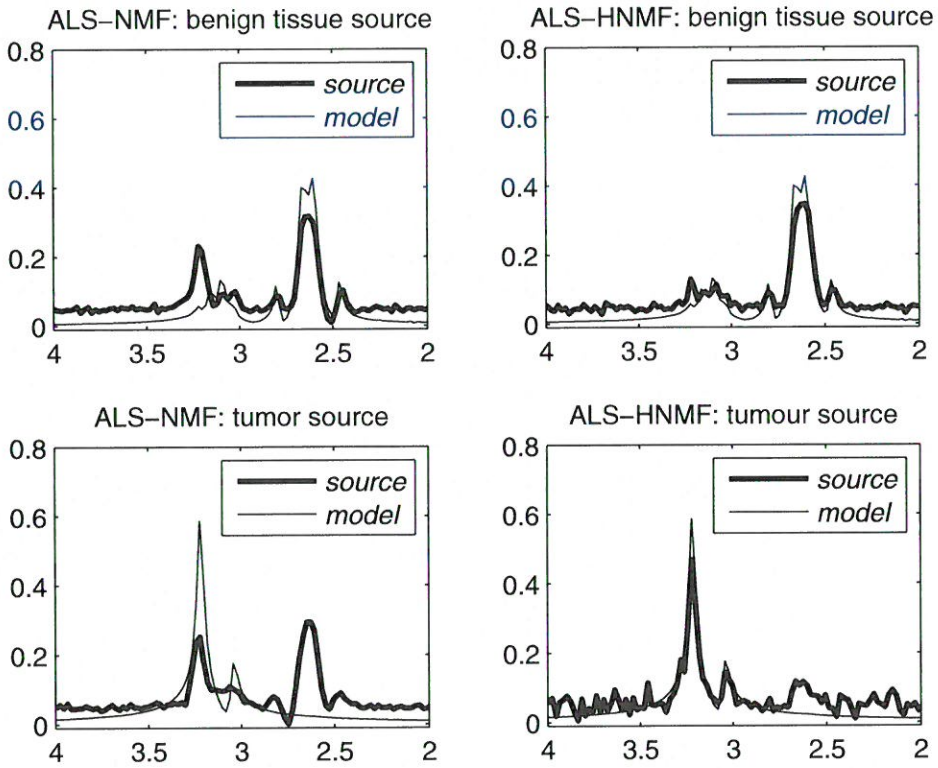


Fig. 7.5 Sources obtained by applying one level of ALS-NMF with $k = 2$ (*left*) and final tissue patterns provided by ALS-HNMF (*right*) superimposed to the theoretical tumour and benign tissue models. The X axis represents frequency values in ppm [14]

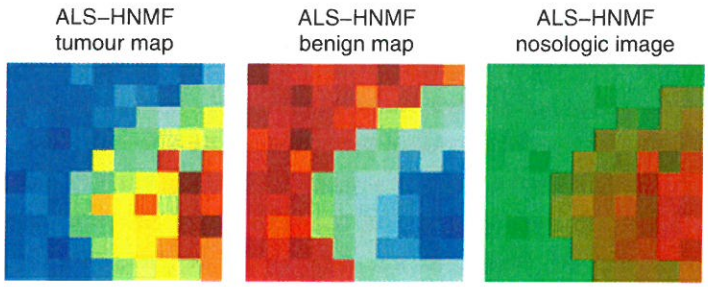


Fig. 7.6 Tissue maps and final nosologic images obtained by NNLS by exploiting the final patterns provided by ALS-HNMF. In the nosologic images, the pathological and benign regions are visualised in *red* and *green*, respectively [14]

In the plots, the patterns are superimposed to the theoretical tumour and benign tissue models. Figure 7.5 clearly shows that the patterns provided by one NMF level (i.e. by ALS-NMF) are very close to each other in shape and both of them represent more mixed tissue than tumour or benign tissue. On the contrary, the tissue patterns obtained by applying the hierarchical approach (ALS-HNMF) are of higher quality as they are very close to the theoretical models represented by the spectra in Fig. 7.3.

Figure 7.6 shows the tissue maps and corresponding nosologic images obtained by applying NNLS between the final tissue patterns obtained by ALS-HNMF and the data matrix X. In the nosologic image (right image), the pathological region is visualised in red and it matches well to that one displayed in the right image of Fig. 7.4, confirming the high degree of accuracy of the proposed NMF-based tissue characterisation approach.

7.5 Conclusions and Future Directions

In this chapter, several NMF-based methods representing the state-of-art in the field of tissue pattern detection and classification of brain and prostate MRS(I) data have been outlined. In particular, algorithms for the recovery of constituent spectra in ex vivo and in vivo brain MRS data, for brain tissue pattern differentiation and for automatic detection and visualisation of prostate tumours using MRSI data, have been described.

All these methods show that NMF is able to extract accurate characteristic tissue patterns from the considered data without the need of any prior tissue model and without imposing strong statistical constraints, such as mutual independence and/or uncorrelation among sources. Furthermore, when considering MRSI data, a fast and automatic visualisation of the pathological area is possible by applying NNLS between the final tissue patterns obtained by NMF and the given data matrix. This approach allows to overcome some of the main limitations that still affect most tissue segmentation and classification techniques of MRS(I) data available in the literature. Indeed, nowadays, the analysis of such data is mainly aimed at building the so-called metabolite maps, and images in which the concentrations of the

t.laudadio@ba.iac.cnr.it

most relevant metabolites are displayed. Unfortunately, the estimation of metabolite concentrations, known as MRS(I) quantification [37–39], is still difficult as MRS(I) spectra are generally affected by noise, artefacts and overlapping peaks, and several time-demanding and user-dependent pre-processing steps are needed before any accurate quantification method could be applied. On the contrary, NMF is very efficient as it requires computational times of the order of a few seconds to extract the desired tissue patterns, and, furthermore, it does not require massive MRS(I) data pre-processing aimed at removing uninteresting spectral components since these are detected as separate sources. Nevertheless, some open problems still characterise the application of NMF to MRS(I) data and their solution represents a difficult but crucial task in order to introduce MRS(I) in routine clinical practice. For instance, as described in Sect. 7.2, the minimisation of (7.1) does not admit unique solution and, therefore, a multiplicity of NMF algorithms is proposed in the literature. Indeed, in the methods described in Sects. 7.3–7.5, different NMF implementations were applied to process the MRS(I) data under investigation and, in some studies, their performance was compared in terms of accuracy. The results show that different implementations could provide different results, but the conclusions of the above studies are only limited to the specific considered implementations and applications, while it would be interesting to carry out a comparative study aimed at assessing whether and which NMF algorithm performs best when applied to any kind of MRS(I) dataset.

A second issue consists in the choice of the optimal k value, representing the number of sources to extract when applying NMF. In most of the MRS(I) applications reported above, such a choice is based on a visual inspection of the sources obtained when applying the method with different k values. More precisely, starting from $k = 2$, k is gradually increased until representative tissue patterns are identified among the extracted sources and, at the same time, further increasing its value only provides redundant information. Although fast, the above approach requires a lot of expertise and user interaction. Currently, other selection criteria are under investigation aimed at providing the optimal value to assign to k automatically.

Finally, an important open problem is represented by the choice of the NMF levels to include in the hierarchical approaches proposed in [10, 14]. As for k, an automatic and, possibly, application-independent procedure would be desirable rather than the heuristic one currently adopted in the aforementioned studies [40].

Solving the above issues would make the application of NMF to MRS(I) data fully unsupervised and automatic, thereby representing an important achievement in the field of MRS(I) data tissue typing for non-invasive diagnosis of cancer.

Besides the aforementioned issues, a possible future research topic is represented by the inclusion of spatial information. Indeed, as described in the Introduction, MRSI provides biochemical information as well as spatial information about the sample under investigation and a natural assumption is that neighbour voxels contain similar tissue types. Previous studies carried out on other algorithms [41, 42] already showed that the simultaneous exploitation of the two types of information significantly improves the performance of the considered methods. Hence, it is reasonable to expect similar improvements by introducing spatial information in the NMF-based algorithms as well.

t.laudadio@ba.iac.cnr.it

Another interesting topic could be represented by the application of NMF to multi-parametric MR data, where information are extracted by making use of more MR modalities (e.g. MRI, MRSI, perfusion-weighted imaging and diffusion-weighted imaging), and properly combined in terms of feature vectors. Also in this case, previous studies showed that exploiting multi-modal information yields more accurate segmentation and classification results [43]. Recently, an interesting unsupervised NMF-based approach has been proposed in [44], where MRI and MRSI data information are simultaneously exploited for detecting brain abnormalities. In conclusion, embedding spatial as well as multi-modal information into NMF would further improve the degree of reliability of the results and, therefore, would make the application of MRS(I) possible in routine clinical practice for diagnosis, monitoring and therapy planning purposes.

Acknowledgments The work of Teresa Laudadio is partly supported by the following projects: PRIN 2012 entitled SMaSIP (Structured matrices in Signal and Image Processing) and Progetto Premiale MIUR 2012 entitled MATHTECH.
The work of Yuqian Li is supported by Young Scientists Fund of the National Natural Science Foundation of China (Grant No. 61401068) and by the China Postdoctoral Science Foundation (Grant No. 2014M552341).
The work of Anca Croitor, Nicolas Sauwen, Diana Sima and Sabine Van Huffel is supported by Research Council KUL: GOA/10/09 MaNet, CoE PFV/10/002 (OPTEC); PhD/Postdoc grants. Flemish Government: FWO: projects: G.0427.10N (Integrated EEG-fMRI), G.0108.11 (Compressed Sensing) G.0869.12N (Tumor imaging) G.0A5513N (Deep brain stimulation); PhD/Postdoc grants; IWT: projects: TBM 080658-MRI (EEG-fMRI), TBM 110697-NeoGuard; PhD/Postdoc grants; iMinds Medical Information Technologies SBO 2014, ICON: NXT_Sleep; Flanders Care: Demonstratieproject Tele-Rehab III (2012–2014). Belgian Federal Science Policy Office: IUAP P7/19/(DYSCO, 'Dynamical systems, control and optimization', 2012–2017). Belgian Foreign Affairs-Development Cooperation: VLIR UOS programmes. EU: The research leading to these results has received funding from the European Research Council under the European Union's Seventh Framework Programme (FP7/2007–2013)/ERC Advanced Grant: BIOTENSORS (no. 339804). This paper reflects only the authors' views and the Union is not liable for any use that may be made of the contained information. Other EU funding: RECAP 209G within INTERREG IVB NWE programme, EU MC ITN TRANSACT 2012 (no. 316679), ERASMUS EQR: Community service engineer (no. 539642-LLP-1-2013).

References

1. S. Nelson, Multivoxel magnetic resonance spectroscopy of brain tumors. Mol. Cancer Ther. **2**(5), 497–507 (2003)
2. X. Leclerc, T. Huisman, A. Sorensen, The potential of proton magnetic resonance spectroscopy (1H-MRS) in the diagnosis and management of patients with brain tumors. Curr. Opin. Oncol. **14**, 292–298 (2002)
3. B. Pickett, J. Kurhanewicz, F. Coakley, K. Shinohara, B. Fein, M. Roach, Use of MRI and spectroscopy in evaluation of external beam radiotherapy for prostate cancer. Int. J. Radiat. Oncol. Biol. Phys. **60**(4), 1047–1055 (2004)
4. L. Kwock, J.K. Smith, M. Castillo, M.G. Ewend, F. Collichio, D.E. Morris, T.W. Bouldin, S. Cush, Clinical role of proton magnetic resonance spectroscopy in oncology: brain, breast, and prostate cancer. Lancet Oncol. **7**(10), 859–868 (2006)

t.laudadio@ba.iac.cnr.it

5. S.J. Nelson, Magnetic resonance spectroscopic imaging. IEEE Eng. Med. Biol. **23**, 30–39 (2004)
6. D.D. Lee, H.S. Seung, Learning the parts of objects by non-negative matrix factorization. Nature **401**, 788–791 (1999)
7. A.R. Croitor Sava, C.M. Martinez-Bisbal, D.M. Sima, J. Calvar, V. Esteve, B. Celda, U. Himmelreich, S. Van Huffel, Quantifying brain tumor tissue abundance in HR-MAS spectra using non-negative blind source separation techniques. J. Chemom. **26**(7), 406–415 (2012)
8. S. Ortega-Martorell, P.J.G. Lisboa, Julià-Sapé M. Vellido, C. Arús, Nonnegative matrix factorisation methods for the spectral decomposition of MRS data from human brain tumours. BMC Bioinform. **13**, 38 (2012)
9. S. Ortega-Martorell, P.J. Lisboa, A. Vellido, R.V. Simões, M. Pumarola, M. Julià-Sapé, C. Arús, Convex non-negative matrix factorization for brain tumor delimitation from MRSI data. PLoS ONE **7**(10), e4 (2012)
10. P. Sajda, S. Du, T.R. Brown, R. Stoyanova, D.C. Shungu, X. Mao, L.C. Parra, Nonnegative matrix factorization for rapid recovery of constituent spectra in magnetic resonance chemical shift imaging of the brain. IEEE Trans. Med. Imaging **23**, 1453–1465 (2004)
11. Y. Li, D.M. Sima, S. Van Cauter, A.R. Croitor Sava, U. Himmelreich, Y. Pi, S. Van Huffel, Hierarchical non-negative matrix factorization (hNMF): a tissue pattern differentiation method for glioblastoma multiforme diagnosis using MRSI. NMR Biomed. **26**(3), 307–319 (2013)
12. Y. Li, D.M. Sima, S. Van Cauter, A.R. Croitor Sava, U. Himmelreich, Y. Pi, Y. Liu, S. Van Huffel, Unsupervised nosologic imaging for glioma diagnosis. IEEE Trans. Biomed. Eng. **60**(6), 1760–1763 (2013)
13. A.R. Croitor Sava, A. Wright, D.M. Sima, T. Laudadio, S. Van Huffel, A. Heerschap, U. Himmelreich, Automatic magnetic resonance spectroscopic imaging segmentation using blind source separation techniques. Lirias number: 421620, in *Proceedings ESMRMB 2013*, Toulouse, October 2013, pp. 330–331
14. T. Laudadio, A.R. Croitor Sava, D.M. Sima, A. Wright, A. Heerschap, S. Van Huffel, Hierarchical non-negative matrix factorization applied to in vivo 3T MRSI prostate data for automatic detection and visualization of tumours. Lirias number: 421618, in *Proceedings ESMRMB 2013*, Toulouse, October 2013, pp. 474–475
15. G.H. Golub, C.F. Van Loan, *Matrix Computations*, 4th edn. (The Johns Hopkins University Press, Baltimore, 2013)
16. H. Laurberg, M.G. Christensen, M.D. Plumbley, L.K. Hansen, S.H. Jensen, Theorems on positive data: on the uniqueness of NMF. Comput. Intell. Neurosci. 764206 (2008). doi:10.1155/2008/764206
17. M.W. Berry, M. Browne, A.N. Langville, V.P. Pauca, R.J. Plemmons, Algorithms and applications for approximate nonnegative matrix factorization. Comput. Stat. Data Anal. **52**, 155–173 (2007)
18. M.C. Martínez-Bisbal, L. Martí-Bonmatí, J. Piquer, A. Revert, P. Ferrer, J.L. Llácer, M. Piotto, O. Assemat, B. Celda, ^{1}H and ^{13}C HR-MAS spectroscopy of intact biopsy samples ex vivo and in vivo ^{1}H MRS study of human high grade gliomas. NMR Biomed. **17**(4), 191–205 (2004)
19. A.R. Croitor Sava, M.C. Martinez-Bisbal, S. Van Huffel, J.M. Cerda, D.M. Sima, B. Celda, Ex vivo high resolution magic angle spinning metabolic profiles describe intratumoral histopathological tissue properties in adult human gliomas. Magn. Reson. Med. **65**, 320–328 (2011)
20. H. Kim, H. Park, Sparse non-negative matrix factorizations via alternating non-negativity-constrained least squares for microarray data analysis. Bioinformatics **23**(12), 1495–1502 (2007)
21. H. Cha, W.K. Ma, C.Y. Chi, Y. Wang, A convex analysis framework for blind separation of non-negative sources. IEEE Trans. Signal Process. **56**(10), 5120–5134 (2008)
22. M.D. Plumbley, Algorithms for non-negative independent component analysis. IEEE Trans. Neural Netw. **14**(3), 534–543 (2003)
23. R. Meyer, M. Fisher, S. Nelson, T. Brown, Evaluation of manual methods for integration of in vivo phosphorus NMR spectra. NMR Biomed. **1**(3), 131–135 (1988)

t.laudadio@ba.iac.cnr.it

24. L.L. Cheng, I.W. Chang, D.N. Louis, R.G. Gonzalez, Correlation of high-resolution magic angle spinning proton magnetic resonance spectroscopy with histopathology of intact human brain tumor specimens. Cancer Res. **58**(9), 1825–1832 (1998)
25. M. Julià-Sapé, D. Acosta, M. Mier, C. Arús, D. Watson, The interpret consortium: a multi-centre, web-accessible and quality control-checked database of in vivo MR spectra of brain tumour patients. Magn. Reson. Mater. Phys. **19**, 22–33 (2006)
26. A.R. Tate, J. Underwood, D.M. Acosta et al., Development of a decision support system for diagnosis and grading of brain tumours using in vivo magnetic resonance single voxel spectra. NMR Biomed. **19**(4), 411–434 (2006)
27. C. Ding, T. Li, M. Jordan, Convex and semi-nonnegative matrix factorizations. IEEE Trans. Pattern Anal. Mach. Intell. **99**(1), 5555 (2008)
28. I.T. Jolliffe, *Principal Component Analysis* (Springer, New York, 2002)
29. K.S. Opstad, C. Ladroue, B.A. Bell, J.R. Griffiths, F.A. Howe, Linear discriminant analysis of brain tumour (1)H MR spectra: a comparison of classification using whole spectra versus metabolite quantification. NMR Biomed. **20**(8), 763–770 (2007)
30. A. Cichocki, R. Zdunek, S. Amari, Hierarchical ALS algorithms for nonnegative matrix and 3D tensor factorization. Lect. Notes Comput. Sci. **4666**, 169–176 (2007)
31. A. Cichocki, A.H. Phan, Fast local algorithms for large scale nonegative matrix and tensor factorizations. IEICE Trans. Fundam. Electron. Commun. Comput. Sci. **3**, 708–721 (2009)
32. N. Gillis, Nonnegative matrix factorization complexity, algorithms and applications. Ph.D. thesis, Louvan-La-Neuve (2011)
33. Y. Li, D.M. Sima, S. Van Cauter, U. Himmelreich, Y. Pi, S. Van Huffel, Simulation study of tissue type differentiation using non-negative matrix factorization, in *Proceedings of BIOSIGNALS 2012, International Conference on Bioinspired Systems and Signal Processing*, Vilamoura, Algarve, February 2012, pp. 212–217
34. F.A. Howe, S.J. Barton, S.A. Cudlip, M. Stubbs, D.E. Saunders, J.R. Murphy, K.S. Opstad, V.L. Doyle, M.A. McLean, B.A. Bell, J.R. Griffiths, Metabolic profiles of human brain tumours using quantitative in vivo 1H magnetic resonance spectroscopy. Magn. Reson. Med. **49**, 223–232 (2003)
35. C.L. Lawson, *Solving Least-Squares Problems*, vol. 23 (Prentice-Hall, Englewood Cliffs, 1974), p. 161
36. K.M. Selnaes, I.S. Gribbestad, H. Bertilsson, A. Wright, A. Angelsen, A. Heerschap, M.B. Tessem, Spatially matched in vivo and ex vivo MR metabolic profiles of prostate cancer-investigation of a correlation with Gleason score. NMR Biomed. **26**(5), 600–606 (2013)
37. S.W. Provencher, Estimation of metabolite concentrations from localized in vivo proton NMR spectra. Magn. Reson. Med. **30**(6), 672–679 (1993)
38. J.B. Poullet, D.M. Sima, A.W. Simonetti, B. De Neuter, L. Vanhamme, P. Lemmerling, S. Van Huffel, An automated quantitation of short echo time MRS spectra in an open source software environment: AQSES. NMR Biomed. **20**(5), 493–504 (2007)
39. J.B. Poullet, D.M. Sima, S. Van Huffel, MRS signal quantitation: a review of time- and frequency-domain methods. J. Magn. Reson. **195**, 134–144 (2008)
40. N. Gillis, D. Kuang, H. Park, Hierarchical clustering of hyperspectral images using rank-two nonnegative matrix factorization (2013). arXiv preprint arXiv:1310.7441
41. T. Laudadio, P. Pels, L. De Lathauwer, P. Van Hecke, S. Van Huffel, Tissue segmentation and classification of MRSI data using canonical correlation analysis. Magn. Reson. Med. **54**, 1519–1529 (2005)
42. A.R. Croitor Sava, D.M. Sima, J.B. Poullet, A.J. Wright, A. Heerschap, S. Van Huffel, Exploiting spatial information to estimate metabolite levels in two-dimensional MRSI of heterogeneous brain lesions. NMR Biomed. **24**(7), 824–835 (2011)
43. M. De Vos, T. Laudadio, A.W. Simonetti, A. Heerschap, S. Van Huffel, Fast nosologic imaging of the brain. J. Magn. Reson. **184**, 292–301 (2006)
44. X. Liu, Y. Li, Y. Pi, S. Van Cauter, Y. Yao, J. Wang, A new algorithm for the fusion of MRSI & MRI on the brain tumour diagnosis, in *Proceedings ISMRM 2015*, Toronto, Ontario, 30 May–5 June 2015

t.laudadio@ba.iac.cnr.it